Chemical Science

ROYAL SOCIETY OF CHEMISTRY

EDGE ARTICLE

View Article Online
View Journal | View Issue

Cite this: *Chem. Sci.*, 2021, **12**, 6136

All publication charges for this article have been paid for by the Royal Society of Chemistry

Modulation of solid surface with desirable under-liquid wettability based on molecular hydrophilic–lipophilic balance†

Yang Wang, [ad] Qifei Wang, [a] Baixian Wang,[a] Ye Tian,[c] Jiancheng Di, *[a] Zuankai Wang, [d] Lei Jiang [c] and Jihong Yu *[ab]

Received 9th February 2021
Accepted 11th March 2021

DOI: 10.1039/d1sc00808k

rsc.li/chemical-science

There has been great interest in the fabrication of solid surfaces with desirable under-liquid wettability, and especially under-liquid dual-lyophobicity, because of their potential for widespread use. However, there remains the lack of a general principle to modulate the under-liquid wettability in terms of surface energy (SE). Herein, we found that the relative proportion between the polar and dispersive components in SE that reflects the competition between hydrophilicity and lipophilicity governs the under-liquid wettability of the solid surface. For the first time, we introduced hydrophilic–lipophilic balance (HLB) calculated solely based on the amount and type of hydrophilic and lipophilic fragments in surface molecules to rapidly predict the under-liquid wettability of a solid surface, thereby guiding the fabrication of solid surfaces with desirable under-liquid wettability. Accordingly, the under-liquid dual superlyophobic surfaces in a nonpolar oil–water-solid system were fabricated by grafting molecules with appropriate HLB values (*e.g.*, 6.341–7.673 in a cyclohexane–water–solid system) onto porous nanofibrous membranes, which were able to achieve continuous separation of oil–water mixtures. This work provides reasonable guidance for the fabrication of solid surfaces with targeted under-liquid wettability, which may lead to advanced applications in oil–water–solid systems.

1. Introduction

Inspired by the unique wetting phenomena found in nature,[1–3] various lyophobic or lyophilic solid surfaces have been developed for the applications of liquid repellence,[4–7] transportation[8,9] or separation,[10–14] anti-fogging,[15] anti-biofouling,[16,17] catalysis,[18,19] and heat transfer.[20,21] In particular, there has been growing interest in the rational modulation of under-liquid wettability of solid surfaces, and especially the achievement of under-liquid dual-lyophobicity, to meet the requirements of environment- and energy-related applications.[22–26] Thus far, there have only been a few studies on wetting mechanisms to guide the modulation of under-liquid wettability. Tian *et al.* proposed that in an oil–water–solid system, the sum of the water contact angle in oil ($\theta_{w/o}$) and the oil contact angle in water ($\theta_{o/w}$) on a thermodynamically stable surface should be 180° in principle because the angles were supplementary to each other. Therefore, the under-liquid dual-lyophobic surface should be metastable in thermodynamics because both $\theta_{w/o}$ and $\theta_{o/w}$ on it were more than 90°.[27] The author also noted that the re-entrant geometric characteristic and the appropriate surface chemical composition were the key factors for realizing under-liquid dual superlyophobicity.

Our previous work demonstrated the rational modulation of the under-liquid wettability of rough surfaces by changing the surface chemical composition. We further ascertained the thermodynamic metastability of the under-liquid dual-lyophobic surfaces by calculating the total interfacial energy at the solid–liquid interface. Consequently, in the nonpolar oil–water–solid system, the under-liquid wettability of the rough surfaces could be inferred according to their intrinsic water contact angle (θ_w).[28] Chen's group demonstrated the restructuring behavior of specific surface molecules in different media (*e.g.*, air, water, and oil), that is, the surface molecules would reorient and selectively expose their hydrophilic or lipophilic (oleophilic) parts to enhance the solid–liquid interaction and decrease the total interfacial energy, thereby leading to different wettabilities.[29–31] However, there remains a lack of a general criterion to address the surface composition influence, which allows rapid and qualitative prediction regarding the under-

[a]*State Key Laboratory of Inorganic Synthesis and Preparative Chemistry, College of Chemistry, Jilin University, Changchun 130012, P. R. China. E-mail: jcdi@jlu.edu.cn; jihong@jlu.edu.cn*

[b]*International Center of Future Science, Jilin University, Changchun 130012, P. R. China*

[c]*Key Laboratory of Bio-Inspired Materials and Interfacial Science, Technical Institute of Physics and Chemistry, Chinese Academy of Sciences, Beijing 100190, P. R. China*

[d]*Department of Mechanical Engineering, City University of Hong Kong, Hong Kong 999077, P. R. China*

† Electronic supplementary information (ESI) available. See DOI: 10.1039/d1sc00808k

liquid wettabilities solely based on the components of surface molecules.

In terms of the classical Young's equation, surface energies (SEs) governed by surface chemical compositions are commonly used to demonstrate the interfacial interaction between liquids and solid surfaces.[32] However, it was found that the further division of SE into the dispersive component (DSE) and polar component (PSE) based on the types of intermolecular forces was more suitable for evaluating interfacial adhesion and explaining some unique wetting phenomena.[33–37] For instance, our previous work demonstrated that the interaction between solid surfaces with high PSE and high-PSE liquids was more facile than that with high-SE liquids, forming a robust solid–liquid composite interface that could prevent the intrusion of immiscible low-PSE liquids.[10] Therefore, it is expected that the under-liquid wettabilities of solid surfaces could be rationally modulated by adjusting the relative proportion between PSE and DSE.

In this work, we discovered that in the nonpolar oil–water–solid systems, the ratio of PSE to DSE, denoted as f, was an appropriate factor to describe the under-liquid wettability of solid surfaces: a lower f value tended denote under-water lipophilicity, whereas a higher f value led to under-oil hydrophilicity. Significantly, when the f value was located in a suitable range, the PSE–PSE and DSE–DSE interfacial interactions maintained their relative balance, resulting in under-liquid dual-lyophobicity.

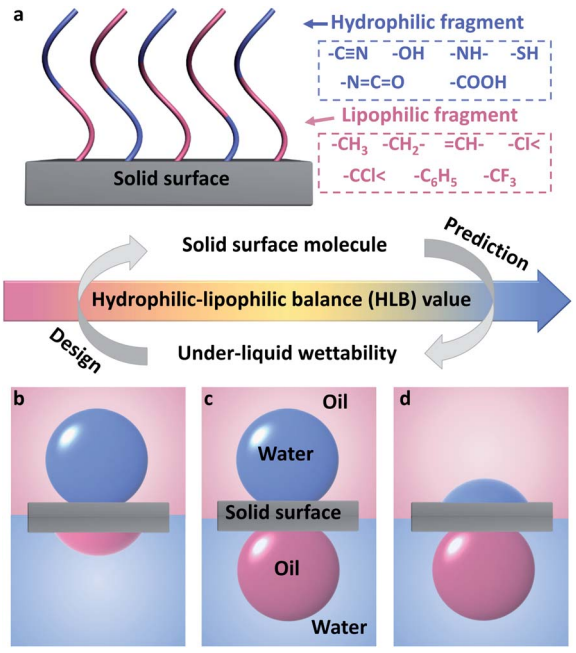

Fig. 1 Schematic illustration of the molecular HLB criterion for rapidly predicting the under-liquid wettability of a solid surface based on the components of surface molecules as well as guiding the fabrication of the solid surface with desirable under-liquid wettability. (a) Solid surface molecule composed of hydrophilic and lipophilic fragments. (b–d) Under-liquid wettability of solid surfaces: (b) under-water lipophilicity/under-oil hydrophobicity, (c) under-liquid dual-lyophobicity, and (d) under-water lipophobicity/under-oil hydrophilicity.

Here, for the first time, we introduce the concept of hydrophilic–lipophilic balance (HLB) to predict the under-liquid wettability of a given surface and guide the fabrication of a solid surface with desirable under-liquid wettability. The HLB value was calculated based on the type and the amount of hydrophilic and lipophilic fragments in the surface molecules (Fig. 1a).[38,39]

We found that in the nonpolar oil–water–solid system, when the HLB value increased, the solid surface was more hydrophilic, and the under-liquid wettability changed in turn, including under-water lipophilicity (oleophilicity)/under-oil hydrophobicity (Fig. 1b), under-liquid dual-lyophobicity (Fig. 1c), and under-water lipophobicity (oleophobicity)/under-oil hydrophilicity (Fig. 1d). Furthermore, under-liquid superlyophobic surfaces were successfully fabricated by grafting surface molecules with appropriate HLB values onto rough substrates *via* a simple chemical modification process. Among them, the representative cyanopropyl-terminated porous nanofibrous membrane efficiently separated layered oil–water mixtures and surfactant-stabilized emulsions.

2. Results and discussion

2.1 Under-liquid wettabilities of solid surfaces with different components of SEs

The surface wettability is determined by the surface topography and the chemical composition. To eliminate the effect of surface geometry on the under-liquid wettability of solid surfaces, smooth silica wafers were used as the substrates on which 14 different molecules were grafted *via* a covalent modification or plasma process (Table S1†). The total SEs of these surfaces, as well as the polar (PSE) and dispersive (DSE) components in the SEs, were estimated based on the contact angle (CA) data and fitted using the OWRK (Owen, Wendt, Rabel, and Kaelble) method (Table S2 and Note S1†).[36,40] Fig. S1† shows four representative fitted curves of glycidyloxypropyl-, methacrylate-, and phenyl-terminated surfaces, and a polydopamine-coated surface. The well-matched fitting curves indicate that the OWRK method is reasonable and adequate to evaluate SE components, and the results are listed in Table S3.† The under-liquid wettabilities of the surfaces with different SEs were investigated in the nonpolar oil–water–solid systems. Taking the cyclohexane–water–solid system as an example, we measured the oil contact angle ($\theta_{o/w}$) and water contact angle ($\theta_{w/o}$) of these surfaces when they were immersed in water and oil, respectively (Table S4†). Fig. 2a shows that the under-water lipophilic surfaces (red dots) and under-liquid dual-lyophobic surfaces (yellow dots), especially for the glycidyloxypropyl- and iodopropyl-terminated surfaces, are overlapped with the increase in SE, suggesting that the under-liquid wettabilities of the solid surfaces cannot be accurately described using the SE as the parameter.

It is known that the polar–polar and dispersive–dispersive interfacial attractions at the solid–liquid interface can be treated independently, which leads to the hydrophilicity and lipophilicity of solid surfaces, respectively. Herein, the ratio of PSE to DSE of the material surface, denoted as f, was employed

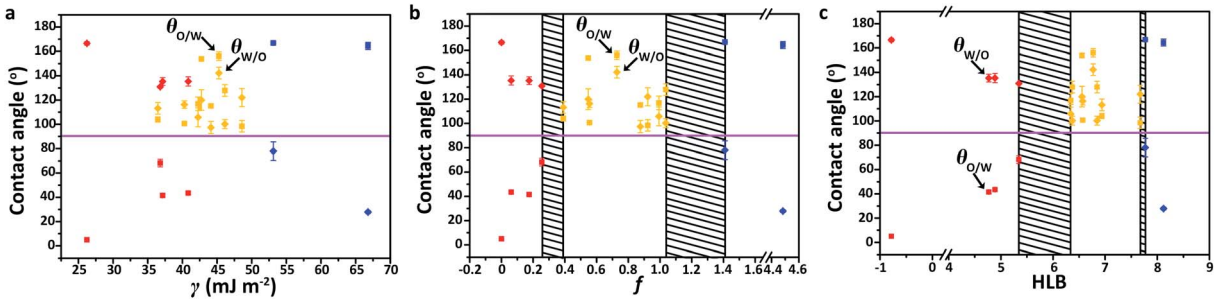

Fig. 2 Under-liquid wettabilities of solid surfaces with different surface molecules. (a) Relationship between under-liquid wettabilities of solid surfaces and their total SEs. No intact region corresponding to the under-liquid dual-lyophobicity is observed. (b) Relationship between under-liquid wettabilities of solid surfaces and their *f* values. The under-liquid wettability of solid surfaces can be divided into three separate regions based on their *f* values. (c) Relationship between under-liquid wettabilities of solid surfaces and their HLB values. The under-liquid wettability of solid surfaces can also be classified into three independent regions according to their HLB values. The shadows in (b) and (c) are attributed to the lack of suitable modulations of surfaces with *f* values in the ranges of 0.254–0.390 and 1.037–1.410, and HLB values in the ranges of 5.346–6.341 and 7.673–7.770, respectively. Note: ■: $\theta_{o/w}$, ◆: $\theta_{w/o}$, red: under-water lipophilicity and under-oil hydrophobicity, yellow: under-liquid dual-lyophobicity, blue: under-water lipophobicity and under-oil hydrophilicity.

as a new parameter to demonstrate the competitive affinity interaction of the solid surface between water and oil. In Fig. 2b, the under-liquid wettabilities of the surfaces can be successfully classified into three separate regions according to their *f* values: (1) $f \leq 0.254$ (red dots), and the DSE-dominated SE affords the surfaces more affinity to oil, showing under-water lipophilicity/under-oil hydrophobicity; (2) $0.390 \leq f \leq 1.037$ (yellow dots), and moderate affinity of the surfaces to both water and oil leads to under-liquid dual-lyophobicity; (3) $f \geq 1.410$ (blue dots), and the higher PSE content in SE results in under-water lipophobicity/under-oil hydrophilicity. Therefore, the under-liquid wettability of solid surfaces can be described more accurately using the *f* value rather than by the total SE. There are two black shadows in Fig. 2b because of the lack of modified surfaces with *f* values in the ranges of 0.254–0.390 and 1.037–1.410.

We then explored the effect of the *f* value on the under-liquid wettability in terms of the solid–liquid interface interaction. In the OWRK method, the interface interaction, called adhesion work (W_a), can be expressed as the following equation:[36,40]

$$W_a = W_a^d + W_a^p = 2\left(\sqrt{\gamma_S^d\gamma_L^d} + \sqrt{\gamma_S^p\gamma_L^p}\right) \quad (1)$$

where W_a^d and W_a^p denote the adhesion work generated by the DSE–DSE and PSE–PSE interfacial attraction, respectively. γ_S^d, γ_S^p, and γ_L^d, γ_L^p represent the DSE and PSE of a solid surface and the liquid, respectively. As shown in Note S2,† the competitive affinity to the solid surface between water and nonpolar oil can be expressed as the ratio of W_a at the water–solid interface (W_{asw}) to that at the oil–solid interface (W_{aso}):

$$W_{asw}/W_{aso} \approx 0.929\left(1 + \sqrt{2.34f_S}\right) \quad (2)$$

where f_S denotes the *f* value of the solid surface. Therefore, the ratio of W_{asw} to W_{aso} is proportional to the square root of the f_S value. Specifically, solid surfaces with higher f_S values exhibit stronger interfacial affinity to water; conversely, lower f_S values denote a stronger interfacial affinity to oil. This result further verifies that the ratio of PSE to DSE can accurately reflect the competitive relationship between hydrophilicity and lipophilicity of a solid surface, and determines the under-liquid wettability in a nonpolar oil–water–solid system.

2.2 The relationship between the hydrophile–lipophile balance (HLB) values and the under-liquid wettabilities

To rapidly and conveniently predict the under-liquid wettabilities, we introduced the concept of hydrophilic–lipophilic balance (HLB) based on the components of surface molecules, which is widely used to evaluate the emulsifying and solubilizing properties of surfactants.[39] Herein, the modified molecules outside the silicon atoms that govern the surface chemical compositions of silica wafers were divided into hydrophilic fragments and the hydrophobic fragments, which were chosen for calculating the HLB values. The equation is expressed as:

$$\mathrm{HLB} = 7 + \sum(\text{hydrophilic group number}) + \sum(\text{lipophilic group number}) \quad (3)$$

where the HLB group number of the surface molecules is calculated by the following equation:[41,42]

$$\text{HLB group number} = -0.337 \times 10^5 \times V_x + 1.5n \quad (4)$$

where V_x denotes the atomic volume data (Table S5†), and *n* relates to the number of water molecules participating in the solvation of different types of surface fragments. The calculated group numbers of lipophilic fragments (*e.g.*, –CF_3, =CH–, and –CH<) and hydrophilic fragments (*e.g.*, –$NHCONH_2$, –C≡N, and –N=C=O) are listed in Tables S6 and S7,† which are generally less and greater than zero, respectively.[41,42] Accordingly, the calculated HLB values of these surfaces are given in Table S8.† When combining the HLB values of these surfaces with their under-liquid wettabilities (Table S4†), the $\theta_{o/w}$ increases with the increase in the HLB value (square in Fig. 2c) in the cyclohexane–water–solid system; in contrast, the $\theta_{w/o}$ decreases (rhombus in Fig. 2c). Therefore, we propose an HLB-based

criterion for predicting the under-liquid wettabilities of solid surfaces: (1) HLB ≤ 5.346 (red dots), and the presence of abundant lipophilic fragments results in under-water lipophilicity/under-oil hydrophobicity; (2) 6.341 ≤ HLB ≤ 7.673 (yellow dots), and the similar affinity of the surface to oil and water leads to under-liquid dual-lyophobicity; (3) HLB ≥ 7.770 (blue dots), and the solid surfaces possess more hydrophilic fragments, thereby demonstrating under-water lipophobicity/under-oil hydrophilicity. The black shadows in Fig. 2c appear due to the lack of modified surface molecules with HLB values in the ranges of 5.346–6.341 and 7.673–7.770, respectively.

The applicability of the HLB-based criterion to the prediction of the under-liquid wettability in other nonpolar oil–water–solid systems was also tested. Fig. S2† provides the $\theta_{w/o}$ and $\theta_{o/w}$ of these modified surfaces in the hexadecane–water–solid system. The under-liquid wettability of surfaces can also be divided into three independent regions, and the boundary is the same as that in the cyclohexane–water–solid system, which is caused by the similar PSE and DSE components of hexadecane to that of cyclohexane. In addition, the HLB values of some reported smooth solid surfaces with known chemical compositions (*e.g.*, hydroxyl-, cyanopropyl-, perfluorooctyl-, perfluorodecyl-, octadecyl-, and SU8-terminated surfaces, as well as polydopamine-coated surfaces) were calculated.[24,27]

In Table S9,† all the calculated results are in good agreement with the experimental results, indicating that the HLB-based criterion can reasonably predict the under-liquid wettability of a given surface. Unfortunately, the HLB theory might be unsuitable for calculating the values of surface molecules containing ionic groups because the *n* values are defined as 9 and 6 for anionic and cationic groups, respectively, leading to extremely high HLB values.[42] This indicates that such surfaces possess an ultra-high affinity for water, thus demonstrating under-water lipophobicity/under-oil hydrophilicity. Note that the surface grafted by the uncompensated benzenesulfonate (BS^-) group exhibits under-liquid dual-lyophobicity, which goes against the HLB-based criterion.[31] Therefore, in this work, the under-liquid wettability of a solid surface containing only non-ionic surface molecules was discussed.

2.3 Fabrication of under-liquid dual superlyophobic surfaces

According to the Wenzel model, the lyophilicity and lyophobicity of the surfaces can be greatly increased *via* roughening the lyophilic and lyophobic materials, respectively.[43] Herein, two types of rough surfaces with different geometries, (i) a vertical silicon nanowire array (SiNW, Fig. 3a and b) and (ii) a SiO_2–TiO_2 porous nanofibrous membrane (STPNM, Fig. 3c and d), were selected as the substrates on which molecules with HLB values in the under-liquid dual lyophobic range (6.341–7.673, *e.g.*, cyanoethyl-, mercaptopropyl-, and aminopropyl-terminated molecules) were modified to achieve under-liquid dual-superlyophobicity. In Table S10,† both $\theta_{o/w}$ and $\theta_{w/o}$ on these rough surfaces are much larger than those on the smooth surfaces (Table S4†), and almost all of them exhibit under-liquid dual superlyophobicity. Exceptionally, the smaller $\theta_{w/o}$ on the cyanoethyl-terminated SiNW (129.6 ± 5.8°) may be

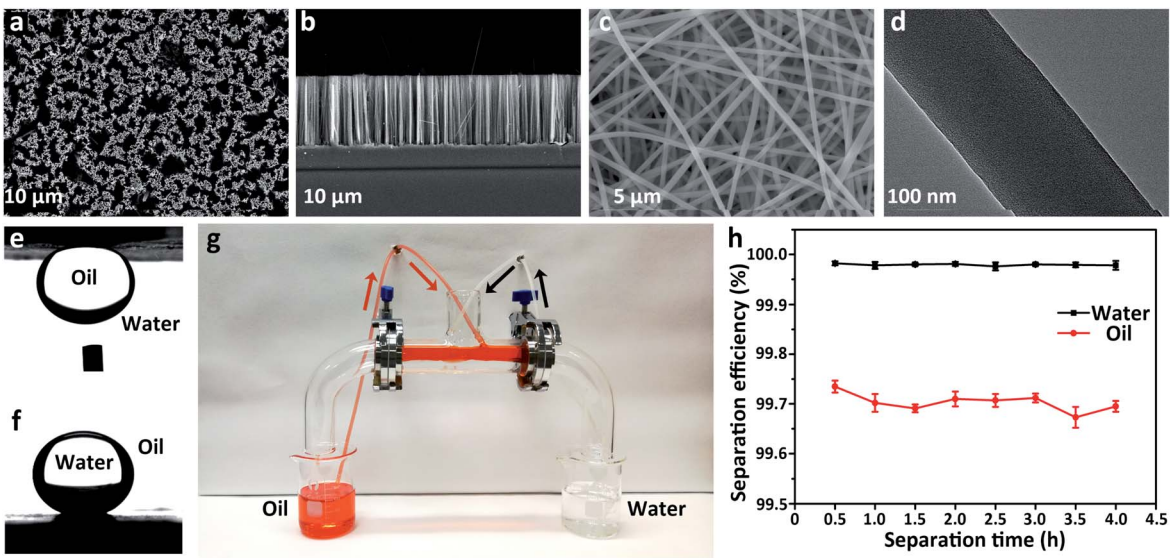

Fig. 3 Morphologies of two rough substrates and the separation capacity of the CSTPNM. (a and b) SEM images of SiNWs showing top and side views, respectively, of the randomly arranged vertical silicon nanowires. (c and d) SEM and TEM images of STPNM, respectively, demonstrating the entangled fibers and hierarchical porous structure. (e and f) Profiles of the under-water oil droplet and under-oil water droplet on the CSTPNM, respectively, indicating the under-liquid dual superlyophobicity. (g) Demonstration of continuous oil–water separation. Two CSTPNMs prewetted with oil (cyclohexane, red) and water (colorless) were fixed onto two outlets of a T-shaped dual-channel apparatus. Cooperating with the automatic feeding by a peristaltic pump, cyclohexane/water mixtures could be continuously separated. (h) The separation efficiency of CSTPNM measured during the 4 h separation process. The error bars representing the s.d. were obtained from the test results of at least five replicates.

caused by the vertical microstructure of the SiNW that is not conducive to maintaining the solid–liquid interface that will repel the immiscible liquid.[27] By contrast, the $\theta_{w/o}$ on cyanoethyl-STPNM reaches 151.2 ± 1.5°, suggesting that the network structure composed of the randomly stacked fibers is more beneficial for holding the infused liquid. This result is analogous to the effect of some unique surface topographies, such as re-entrant geometry, on the ability of the surfaces to repel both water and oil in the oil–water–solid or air–liquid–solid system.[6,27]

2.4 The separation capacity of the under-liquid dual superlyophobic membrane

To evaluate the oil–water separation capacity of the under-liquid dual superlyophobic membrane, the cyanopropyl-STPNM (CSTPNM) with $\theta_{o/w}$ of 159.4 ± 2.7° and $\theta_{w/o}$ of 157.4 ± 2.6° (Fig. 3e and f) was used as an example to continuously separate a layered cyclohexane/water mixture. The CSTPNMs were fixed on two outlets of a T-shaped dual-channel apparatus, which were prewetted by a small quantity of water and cyclohexane, realizing the prewetting-triggered under-water superlipophobicity and under-oil superhydrophobicity, respectively (Fig. 3g). The CSTPNM allowed the passage of the infused liquid itself but repelled another liquid. Cooperating with the automatic feeding by the peristaltic pump, a mixture of water (colorless) and cyclohexane (red) could be continuously separated. The separation efficiency was evaluated *via* analysing the residual content of cyclohexane and water in the two collected liquids (Fig. 3h).

The separation efficiencies for both oil and water were greater than 99.5%, and there was no apparent attenuation after a lengthy separation of 4 h.

Furthermore, the surfactant-stabilized emulsions, including the CTAB-stabilized cyclohexane-in-water and SDBS-stabilized water-in-cyclohexane emulsions, were prepared to verify the emulsion separation capacity of CSTPNM. The as-prepared emulsions were milky white, and large amounts of micron-sized droplets were observed in the view (Fig. S3†). After the filtration process, the filtrates of both oil-in-water (separated by the water-prewetted CSTPNM) and water-in-oil (separated by the cyclohexane-prewetted CSTPNM) emulsions became transparent, and the densely-packed droplets in emulsions were entirely removed, indicating the high efficiency of the membranes for separating emulsions.

3. Conclusions

In summary, 14 different surface molecules with different SE components were grafted onto silicon wafers *via* a covalent modification process, giving rise to modulated under-liquid wettabilities such as under-water lipophilicity/under-oil hydrophobicity, under-liquid dual-lyophobicity, and under-water lipophobicity/under-oil hydrophilicity. We found that the ratio of PSE to DSE that reflected the competitive relationship between hydrophilicity and lipophilicity of a solid surface was an appropriate parameter to describe under-liquid wettability. For instance, under-liquid dual-lyophobicity could be realized when PSE–PSE and DSE–DSE interfacial interactions maintained a relative balance. We further introduced an HLB-based criterion for rapidly predicting the under-liquid wettability of a solid surface exclusively based on the type and amount of hydrophilic fragments and hydrophobic fragments in the surface molecule.

We found that surfaces with lower HLB values tended to be more lipophilic. In contrast, surfaces with higher HLB values led to more affinity with water. When the HLB value was located in a suitable range (*e.g.*, 6.341–7.673 in cyclohexane–water-solid system), the under-liquid dual-lyophobicity of a solid surface was achieved. The under-liquid dual superlyophobic surfaces were successfully fabricated by affording proper HLB values onto the electrospun porous nanofibrous membranes, which were able to efficiently separate layered cyclohexane-water mixtures, as well as CTAB-stabilized cyclohexane-in-water and SDBS-stabilized water-in-cyclohexane emulsions. This work provides straightforward guidance for the fabrication of solid surfaces with desirable under-liquid wettability simply based on the components of surface molecules, which may provide new perspectives for applications in oil–water–solid systems, such as liquid separation, liquid–liquid interface assembly, heterogeneous catalysis, controlled bioadhesion, and anti-biofouling.

4. Experimental

4.1 Materials

Titanium(III) chloride (20 wt% in 2 M HCl aqueous solution) was obtained from Acros Organics. Polyethylene oxide (M_w: 1 000 000) and dopamine hydrochloride (99%) were purchased from Alfa Aesar. Absolute ethanol (analytical reagent (A.R.)), acetone (A.R.), tetraethoxysilane (98%, A.R.), hexadecyltrimethylammonium bromide (CTAB), sodium dodecyl benzene sulfonate (SDBS), sulfuric acid (H_2SO_4, A.R.), hydrogen peroxide (H_2O_2, A.R.), hydrofluoric acid (HF, A.R.), silver nitrate ($AgNO_3$, A.R.), nitric acid (A.R.), cyclohexane (A.R.), and hexadecane (A.R.) were purchased from Beijing Fine Chemical Co. Ltd. Tetrachloromethane (CCl_4, for infrared oil measurement) was obtained from Tianjin Kermel Chemical Reagent Co., Ltd.

4.2 Pretreatment of silicon wafers

Silicon wafers (p-type ⟨100⟩-oriented, 10–20 Ω cm) were cut into 1.2 × 1.2 cm pieces and ultrasonically washed in water, ethanol, and then acetone for 30 min. The silicon wafers were treated in a boiling piranha solution ($H_2SO_4 : H_2O_2 = 7 : 3$, v/v) for 1 h on a heating plate (240 °C) in a fume hood, and then thoroughly rinsed with deionized water and dried with a flow of nitrogen.

4.3 Plasma treatment of silicon wafers

The plasma treatment was performed using a PT-03-LF Plasma System for 300 s, with the gas flow of dry air at 20 $cm^3\ min^{-1}$ and forward RF Target power of 65 W.

4.4 Fabrication of polydopamine coatings on silicon wafers

First, 0.8 g of dopamine hydrochloride was completely dissolved in 250 mL aqueous solution (10 mM Tris-buffer, pH 8.5). Then, the silicon wafer was placed into the solution and immediately stirred for 10 h at room temperature. The polydopamine-modified silicon wafer was washed with deionized water and ethanol several times and dried with a flow of nitrogen.

4.5 Fabrication of SiNWs

One piece of a cleaned silicon wafer was immersed into 20 mL aqueous solutions of 5 M HF and 0.02 M $AgNO_3$. After etching for 1 h at 50 °C, the as-prepared SiNW was placed in dilute nitric acid for at least one hour to remove the excess Ag. Then, the SiNW was washed with deionized water and ethanol several times and dried with a flow of nitrogen.

4.6 Fabrication of STPNMs

A total of 6.5 g of ethanol, 5.0 g of titanium(III) chloride, 3.5 g of hexadecyltrimethylammonium bromide, and 0.32 g of polyethylene oxide were mixed with magnetic stirring. Subsequently, 8.3 g of tetraethoxysilane was added, with continuous stirring for 1 h. The precursor solution was electrospun onto an aluminum foil-covered metallic rotating roller with an electrical potential of 25 kV. The as-spun fibers were aged at 110 °C overnight and then calcined at 550 °C in air for 4 h to remove the organics.

4.7 Silanization process

Eight pieces of substrates (silicon wafer, SiNW, or STPNM) with 1.2 × 1.2 cm in size were placed into a closed desiccator containing silanization reagent. Then, the substrates underwent silanization at 150 °C under reduced pressure (0.2 atm) for 2 h. Typically, eight silicon wafer pieces were placed into a 2.0 L desiccator containing 0.2 mL of 3-cyanopropyltriethoxysilane. The pressure in the desiccator was decreased by vacuum to 0.2 atm, and then, the desiccator was placed in an oven at 150 °C for 2 h.

4.8 Characterizations

Contact angles were measured with a Data-Physics OCA20 machine at ambient temperature, and each value was obtained by measuring five different positions. SEM images were recorded using a JSM-6510 microscope. TEM images were obtained with a JEOL JEM-2100F microscope. The oil concentration in the collected water was measured using an OIL480 infrared spectrometer oil content analyzer. The corresponding method consisted of solvent extraction (CCl_4) and infrared spectrophotometry (2930 cm^{-1}, 2960 cm^{-1}, and 3030 cm^{-1}). The water concentration in the collected oil was analyzed by an automated Karl Fischer titrator, Aquamax HTYWS-H. The separation efficiency (%) was calculated by $(1 - C_i/C_c) \times 100$, where C_i and C_c denote the concentration of the oil or water in the initial solution and the collected liquid, respectively. Optical microscopy images were obtained using a BX53M microscope (Olympus).

Author contributions

J. Y. and J. D. conceived and supervised the project. Y. W. designed and carried out the experiments. Q. W. and B. W. performed some of the experiments. Y. W. wrote the manuscript. Y. T., Z. W. and L. J. participated in the discussion, and J. D. and J. Y. revised the manuscript. All authors discussed the results and commented on the manuscript.

Conflicts of interest

There are no conflicts to declare.

Acknowledgements

This work is supported by the National Natural Science Foundation of China (Grant No. 21621001, 21835002, and 21920102005), and the 111 Project (No. B17020).

Notes and references

1 G. Fogg, *Nature*, 1944, **154**, 515.
2 H. F. Bohn and W. Federle, *Proc. Natl. Acad. Sci. U. S. A.*, 2004, **101**, 14138–14143.
3 H. Chen, P. Zhang, L. Zhang, H. Liu, Y. Jiang, D. Zhang, Z. Han and L. Jiang, *Nature*, 2016, **532**, 85–89.
4 T. S. Wong, S. H. Kang, S. K. Y. Tang, E. J. Smythe, B. D. Hatton, A. Grinthal and J. Aizenberg, *Nature*, 2011, **477**, 443–447.
5 X. Deng, L. Mammen, H.-J. Butt and D. Vollmer, *Science*, 2012, **335**, 67–70.
6 T. L. Liu and C. J. Kim, *Science*, 2014, **346**, 1096–1100.
7 D. Wang, Q. Sun, M. J. Hokkanen, C. Zhang, F. Y. Lin, Q. Liu, S. P. Zhu, T. Zhou, Q. Chang, B. He, Q. Zhou, L. Chen, Z. Wang, R. H. A. Ras and X. Deng, *Nature*, 2020, **582**, 55–59.
8 C. Li, N. Li, X. Zhang, Z. Dong, H. Chen and L. Jiang, *Angew. Chem., Int. Ed.*, 2016, **55**, 14988–14992.
9 J. Li, X. Zhou, J. Li, L. Che, J. Yao, G. McHale, M. K. Chaudhury and Z. Wang, *Sci. Adv.*, 2017, **3**, eaao3530.
10 Y. Wang, J. Di, L. Wang, X. Li, N. Wang, B. Wang, Y. Tian, L. Jiang and J. Yu, *Nat. Commun.*, 2017, **8**, 575.
11 R. Qu, X. Li, Y. Liu, H. Zhai, S. Zhao, L. Feng and Y. Wei, *Angew. Chem., Int. Ed. Engl.*, 2020, **59**, 13437–13443.
12 Z. Xue, Y. Cao, N. Liu, L. Feng and L. Jiang, *J. Mater. Chem. A*, 2014, **2**, 2445–2460.
13 Z. Cheng, D. Zhang, X. Luo, H. Lai, Y. Liu and L. Jiang, *Adv. Mater.*, 2020, **33**, 2001718.
14 J. Di, L. Li, Q. Wang and J. Yu, *CCS Chem.*, 2021, **3**, 2280–2297.
15 T. Mouterde, G. Lehoucq, S. Xavier, A. Checco, C. T. Black, A. Rahman, T. Midavaine, C. Clanet and D. Quéré, *Nat. Mater.*, 2017, **16**, 658–663.
16 M. Mrksich and G. M. Whitesides, *Annu. Rev. Biophys. Biomol. Struct.*, 1996, **25**, 55–78.
17 S. Amini, S. Kolle, L. Petrone, O. Ahanotu, S. Sunny, C. N. Sutanto, S. Hoon, L. Cohen, J. C. Weaver,

J. Aizenberg, N. Vogel and A. Miserez, *Science*, 2017, **357**, 668–673.
18 G. Huang, Q. Yang, Q. Xu, S. H. Yu and H. L. Jiang, *Angew. Chem., Int. Ed.*, 2016, **55**, 7379–7383.
19 S. Crossley, J. Faria, M. Shen and D. E. Resasco, *Science*, 2010, **327**, 68–72.
20 D. Arnaldo del Cerro, A. l. G. Marín, G. R. Römer, B. Pathiraj, D. Lohse and A. J. Huis in't Veld, *Langmuir*, 2012, **28**, 15106–15110.
21 I. U. Vakarelski, N. A. Patankar, J. O. Marston, D. Y. Chan and S. T. Thoroddsen, *Nature*, 2012, **489**, 274–277.
22 M. Tao, L. Xue, F. Liu and L. Jiang, *Adv. Mater.*, 2014, **26**, 2943–2948.
23 J. Li, D. Li, Y. Yang, J. Li, F. Zha and Z. Lei, *Green Chem.*, 2015, **18**, 541–549.
24 P. Zhang, S. Wang and L. Jiang, *Small*, 2015, **11**, 1939–1946.
25 P. Zhu, T. Kong, Y. Tian, X. Tang, X. Tian and L. Wang, *Mater. Horiz.*, 2018, **5**, 1156–1165.
26 H. Kang, Y. Liu, H. Lai, X. Yu, Z. Cheng and L. Jiang, *ACS Nano*, 2018, **12**, 1074–1082.
27 X. Tian, V. Jokinen, J. Li, J. Sainio and R. H. Ras, *Adv. Mater.*, 2016, **28**, 10652–10658.
28 Q. Wang, Y. Wang, B. Wang, Z. Liang, J. Di and J. Yu, *Chem. Sci.*, 2019, **10**, 6382–6389.
29 J. Wang, Z. Paszti, M. A. Even and Z. Chen, *J. Am. Chem. Soc.*, 2002, **124**, 7016–7023.
30 J. Wang, S. E. Woodcock, S. M. Buck, C. Chen and Z. Chen, *J. Am. Chem. Soc.*, 2001, **123**, 9470–9471.
31 X. Liu, C. Leng, L. Yu, K. He, L. Brown, Z. Chen, J. Cho and D. Wang, *Angew. Chem., Int. Ed.*, 2015, **54**, 4851–4856.
32 T. Young, *Philos. Trans. R. Soc. London*, 1805, **95**, 65–87.
33 F. M. Fowkes, *J. Phys. Chem.*, 1962, **66**, 382.
34 F. M. Fowkes, *Ind. Eng. Chem.*, 1964, **56**, 40–52.
35 S. Wu, *J. Adhes.*, 1973, **5**, 39–55.
36 D. K. Owens and R. C. Wendt, *J. Appl. Polym. Sci.*, 1969, **13**, 1741–1747.
37 W. Rabel, *Farbe und Lack*, 1971, **77**, 997–1006.
38 W. C. Griffin, *J. Soc. Cosmet. Chem.*, 1949, **1**, 311–326.
39 J. T. Davies and E. K. Rideal, *Interfacial Phenomena*, Academic Press, New York and London, 2nd edn, 1961.
40 D. H. Kaelble, *J. Adhes.*, 1970, **2**, 66–81.
41 J. C. McGowan, *Tenside, Surfactants, Deterg.*, 1990, **27**, 229–230.
42 R. Sowada and J. C. McGowan, *Tenside, Surfactants, Deterg.*, 1992, **29**, 109–113.
43 R. N. Wenzel, *Ind. Eng. Chem.*, 1936, **28**, 988–994.